Journal of ELECTRONIC MATERIALS, Vol. 46, No. 7, 2017
DOI: 10.1007/s11664-017-5363-6

Electric and Dielectric Properties of Au/ZnS-PVA/n-Si (MPS) Structures in the Frequency Range of 10–200 kHz

NALAN BARAZ,[1] İBRAHIM YÜCEDAĞ,[2] YASHAR AZIZIAN-KALANDARAGH,[3,4,9] GÜLÇIN ERSÖZ,[2,5] İKRAM ORAK,[6] ŞEMSETTIN ALTINDAL,[7] BASHIR AKBARI,[3] and HOSSEIN AKBARI[8]

1.—Department of Electric and Energy, Gölyaka Vocational High School, Düzce University, 81800 Düzce, Turkey. 2.—Department of Computer Engineering, Technology Faculty, Düzce University, 81620 Düzce, Turkey. 3.—Department of Physics, University of Mohaghegh Ardabili, P.O. Box 179, Ardabil, Iran. 4.—Department of Engineering Sciences, Sabalan University of Advanced Technologies (SUAT), Namin, Iran. 5.—Department of Computer Programming, Rumeli Vocational High School, Rumeli University, 34570 İstanbul, Turkey. 6.—Vocational School of Health Services, Bingöl University, 12000 Bingöl, Turkey. 7.—Department of Physics, Faculty of Sciences, Gazi University, Ankara, Turkey. 8.—Department of Physics, Ardabil Branch, Islamic Azad University, Ardabil, Iran. 9.—e-mail: yashar.a.k@gmail.com

Pure polyvinyl alcohol (PVA) capped ZnS semiconductor nanocrystals were prepared by microwave-assisted method, and the optical and structural properties of the as-prepared materials were characterized by x-ray diffraction (XRD) and ultraviolet–visible (UV–Vis) techniques. The XRD pattern shows the formation of ZnS nanocrystals, and the UV–Vis spectroscopy results show a blue shift of about 1.2 eV in its band gap due to the confinement of very small nanostructures. The concentration of donor atoms (N_D), diffusion potential (V_D), Fermi energy level (E_F), and barrier height (Φ_B (C–V)) values were obtained from the reverse bias C^{-2}–V plots for each frequency. The voltage dependent profile of series resistance (R_s) and surface states (N_{ss}) were also obtained using admittance and low–high frequency methods, respectively. R_s–V and N_{ss}–V plots both have distinctive peaks in the depletion region due to the spatial distribution charge at the surface states. The effect of R_s and interfacial layer on the C–V and G/ω–V characteristics was found remarkable at high frequencies. Therefore, the high frequency C–V and G/ω–V *plots* were corrected to eliminate the effect of R_s. The real and imaginary parts of dielectric constant (ε' and ε'') and electric modulus (M' and M''), loss tangent (tan δ), and ac electrical conductivity (σ_{ac}) were also obtained using C and G/ω data and it was found that these parameters are indeed strong functions of frequency and applied bias voltage. Experimental results confirmed that the N_{ss}, R_s , and interfacial layer of the MPS structure are important parameters that strongly influence both the electrical and dielectric properties. The low values of N_{ss} ($\sim 10^9$ eV^{-1} cm^{-2}) and the value of dielectric constant (ε' = 1.3) of ZnS-PVA interfacial layer even at 10 kHz are very suitable for electronic devices when compared with the SiO_2. These results confirmed that the ZnS-PVA considerably improves the performance of Au/n-Si (MS) structure and also allow it to work as a capacitor, which stores electric charges or energy.

Key words: Au/ZnS-PVA/n-Si (MPS), electrical and dielectric properties, electric modulus and ac electrical conductivity, frequency and voltage dependence, microwave-assisted method

(Received March 11, 2016; accepted February 8, 2017; published online February 27, 2017)

INTRODUCTION

Over the past few decades, nanomaterials have received enormous scientific attention due to their interesting novelty and improved optical and electrical properties as a result of size reduction to the nano-regime.[1–3] Synthesis and characterization of discrete semiconductor nanostructures is of significant importance because of their fundamental role in basic research and technological applications. Nanosized particles of semiconducting compounds, in particular, display grain size dependent optoelectronic properties, due to the size quantization effects.[4–6] Among the semiconductors, zinc sulphide (ZnS) is an important material due to its unique properties. ZnS is an important II–VI semiconductor material with a wide band gap (3.72 eV for the cubic zincblende phase and 3.77 eV for the hexagonal wurtzite phase at room temperature) with a high index of refraction and a high transmittance in the visible range, and it is one of the more important materials in photonics research.[7–11] ZnS has been used widely in the fields of phosphor in photoluminescence,[12] electroluminescence,[13] actuators,[14] solar cells,[15] sensors,[16] light-emitting diodes,[17] catalysis,[18] lasers,[19] flat-panel displays,[20] field effect transistors,[21] and so on. One of the important applications of ZnS is in the fabrication of Schottky barrier diodes (SBD_S).[22,23] A Schottky diode is a special type of diode with a very low forward-voltage drop and a very fast switching action. When current flows through a diode, there is a small voltage drop across the diode terminal.[24–27] The current transport mechanism depends on various parameters such as the surface preparation process and vacuum technologies, which are sophisticated with the studies of Schottky barrier height (SBH), the presence of an interfacial oxide of dielectric layer, which separates the metal from semiconductor, impurity concentration of a semiconductor density of interface states or defects series resistance, device temperature and bias voltage.[28–31] SBH can be determined using current–voltage (I–V), capacitance–voltage (C–V), photocurrent and x-ray photoelectron spectroscopy (XPS) measurements.[32–34] Many methods such as hydrothermal,[35] sonochemical,[36] thermal evaporation,[37] wet chemical process,[38] solid state,[39] microwave irradiation,[40] solvothermal,[41] chemical bath deposition,[42] and micro-emulsion[43] have been developed for preparation of ZnS nanomaterials. Among these synthesis methods, the microwave assisted method has proven to be a simple method for the production of nanomaterials. Microwave syntheses have the advantage of employing lower reaction times with respect to the other chemical methods. This synthesis method is based on the rapid and uniform heating of materials because of a direct molecular interaction between these ones and the electromagnetic energy of the microwaves.[44,45]

Because of the existence of an insulator or polymer layer between metal and semiconductor, the metal–semiconductor (MS) structure is converted into a metal–insulator–semiconductor (MIS) or metal–polymer–semiconductor (MPS) type structure, which stores dielectric charge by virtue of the dielectric properties of the interfacial layer. In these structures, especially series resistance (R_s), surface states (N_{ss}), the thickness of the interfacial layer and its homogeneities are important parameters that affect both electric and dielectric characteristics.[46–52] In these structures, metal and semiconductor remain separated by an interfacial layer, and there is a continuous distribution of N_{ss} between the semiconductor and interfacial layer. The C–V–f and G–V–f measurements can supply detailed information on the electric and dielectric characteristics of these type of structures. The reasons for the existence of R_s and N_{ss} are the surface preparation, fabrication process, interfacial layer and its homogeny, the concentration of doping atoms, the interruption of the periodic lattice structure, and the stability of polymer used.[48–52]

The aim of this study is to determine and interpret the effects of ZnS-polyvinyl alcohol (PVA) interfacial layer located at M/S interface, surface states, R_s, and possible polarization mechanisms on the electric and dielectric properties of the fabricated Au/ZnS-PVA/n-Si (MPS) structures. ZnS nanostructures were prepared by microwave assisted method in the presence of PVA as a capping agent. Therefore, the frequency and voltage dependent electrical and dielectric properties of the structure were investigated in detail by using the C–V and G/ω–V measurements in the frequency and voltage ranges of 10–200 kHz and ±3 V, respectively.

MATERIALS AND METHODS

Preparation of ZnS Nanostructures

To synthesize zinc sulfide nanostructures the chemicals used were zinc acetate ($(CH_3CO_2)_2Zn{\cdot}2H_2O$), polyvinyl alcohol (PVA), and sodium sulfide ($Na_2S{\cdot}9H_2O$). In a typical procedure, aqueous stock solutions of (0.2 M) 0.87 g of $(CH_3CO_2)_2Zn{\cdot}2H_2O$, was dissolved in 20 mL doubled distilled water; in another beaker 0.48 g $Na_2S{\cdot}9H_2O$ was dissolved in 20 mL of distilled water (0.1 M). The zinc acetate solution was then added to the sodium sulfide solution. This solution was irradiated with a high intensity ultrasonic at room temperature for 15 min using Dr. Heilscher ultrasound processor (UP200H Germany, 14 mm diameter Ti horn, 200 W/cm^2, 24 kHz). PVA was added to the solution with three different concentrations (1%, 3%, and 5%) and the effect of addition was characterized. The prepared suspension was centrifuged to get the precipitate out and washed four times using double distilled water and ethanol to remove the unreacted reagents and dried in an oven at 80°C for 3 h.

Fabrication Process of Au/ZnS-PVA/n-Si Structures

Au/ZnS-PVA/n-Si (MPS) type structures were fabricated on P-doped (n-Si) single Si wafer with (100) orientation, ~300 μm thickness and 1–10 Ω cm resistivity. The n-Si wafer was cleaned at 55°C acetone for 10 min, then was immersed in methanol and rinsed in de-ionized water. After that, the n-Si wafer was etched in a 70°C solution of H_2O, NH_4OH and H_2O_2 (65:13:13 v/v) and rinsed in de-ionized water. Finally n-Si wafer was dried by dry nitrogen gas (N_2). After cleaning processes, n-Si wafer was transferred into the deposition chamber and then the high purity (99.999%) of Au with a thickness of ~1500 Å was thermally evaporated from the tungsten filament onto the whole back side of the n-Si wafer at about 10^{-6} Torr in an oil high vacuum metal evaporation system. In order to obtain a good or low resistivity ohmic contact, the n-Si wafer was annealed at 500°C. Then, the sample was also tested to examine whether or not it has a good ohmic contact behavior. After that the prepared ZnS-doped PVA nanocomposite was deposited on the front surface of n-Si wafer using sol–gel method. Finally, the high purity of Au dots with 1 mm diameter (area = 7.85×10^{-3} cm^{-2}) and ~1500 Å thickness were deposited on the front of ZnS-doped nanocomposite PVA in the same high vacuum system. Thus, the fabrication of Au/ZnS-PVA/n-Si (MPS) type structures was completed. For the measurements of the forward and reverse bias C–V and G/ω–V data, the prepared samples were placed on the Cu-holder with the help of silver paste and the electrical contacts were also made to the upper electrodes using thin silver coated wires with silver paste.

Instrument

Optical absorption studies were carried out using a ultraviolet–visible (UV–Vis) spectrophotometer (Shimadzu). The structural characterization of nanocrystals was carried out by analyzing x-ray diffraction (XRD) patterns, obtained using an Ital-structures (MPD3000) instrument operating at 40 kV and a current of 30 mA with Cu Kα radiation (wavelength = 1.54056 Å). The surface morphology of samples was analyzed using a scanning electron microscope (SEM), LEO, 1430VP at 15 kV accelerating voltage. The C–V and G/ω–V measurements of the structure were performed in the frequency range of 10–200 kHz by using an HP 4192A LF impedance analyzer (5 Hz–13 MHz) at room temperature. The thickness of interfacial layer (d_i) was obtained from the interfacial layer capacitance (C_i ($=\varepsilon'\varepsilon_o A/d_i$) as 51 nm at 200 kHz. All of measurements were carried out with the help of a microcomputer through an IEEE-458 AC/DC converter card.

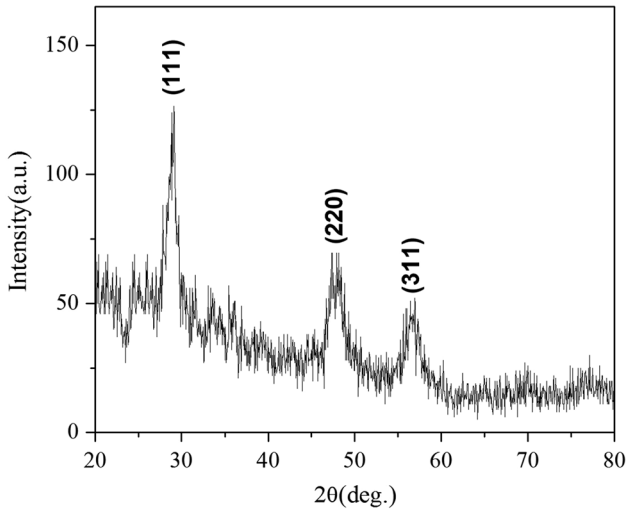

Fig. 1. XRD pattern of as-prepared sample with 5% capping agent concentration.

RESULTS AND DISCUSSION

Structural and Optical Analyses

X-ray Diffraction

The crystal structure of as-prepared sample was examined by XRD analysis. Figure 1 shows the XRD pattern of sample synthesis with the microwave-assisted method with 5% capping agent concentration. The peaks are identified compared to ICDD data; all diffraction peaks can be readily indexed to the ZnS nanostructures; no other peaks were observed, which indicates a sample with high purity.

The broadness of the peaks indicates that the size of structure is reasonably nanocrystalline in nature.

The crystallite size has been examined by the Scherrer formula applied to the (111) orientation which is the maximum intensity reflection of the ZnS structure: $L = 0.9\ \lambda/\beta\cos\theta$,[44] where L is the coherent length, λ is the wavelength of the incident x-ray beam, β is the full-width at half-maximum in radians, and θ is the Bragg's angle. In the case of spherical crystallite, L is given by ¾D. The crystallite size of as-prepared ZnS nanoparticles by use of Sherrer equation was found to be less than 30 nm.

SEM and TEM Analyses

The morphology of the prepared products was studied by scanning electron microscopy (SEM). The SEM image (Fig. 2) shows that the product is consisting of small spherical ZnS nanocrystallites aggregated in the form of polydispersive nanoclusters with sizes smaller than 100 nm. It is very hard to discuss about size of nanoparticles using SEM images, but from images it is clear that the sizes are in the order of very small nanoparticles.

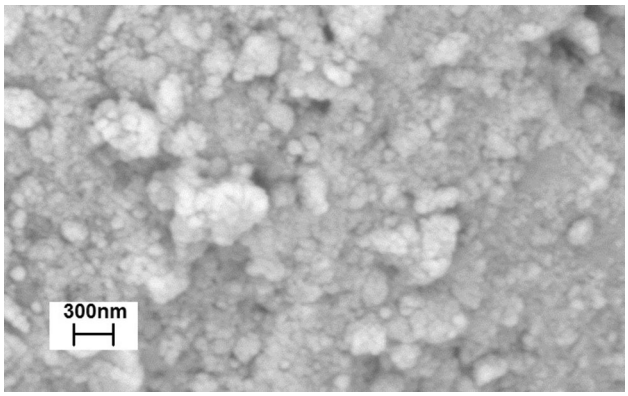

Fig. 2. SEM image of as-prepared sample with 5% of capping agent concentration.

Transmission electron microscopy (TEM) image was taken for a further investigation on the morphology and the size of nanoparticles and the image was given in Fig. 3. Comparison of TEM and SEM images confirms the formation of very small spherical ZnS nanoparticles most of which aggregated together in the form of polydispersive nanoclusters.

UV–Vis Spectroscopy

The optical properties of the as-prepared sample were studied in the wavelength region of 200–800 nm, and the optical band gap was calculated for the sample.

The optical absorbance edge of ZnS sample was blue shifted from that of the bulk form (329 nm, E_g = 3.77 eV). The broadening of the absorbance spectrum was increasing capping agent due to the quantum confinement of nanostructures. Optical band gap was evaluated from the absorption spectrum and optical coefficient (α) near the absorption edge is given by:

$$(\alpha h\nu)^{1/2} = (E_g - h\nu) \quad (1)$$

where α, ν, and E_g are the absorption coefficient, the light frequency, the band gap and a constant, respectively.[11] The corresponding band gap energy for as-prepared sample was calculated as 4.95 eV, obviously blue shifted in comparison with the bulk form.

Electrical and Dielectric Analyses

Capacitance–Voltage Characteristics

Experimental C–V and G/ω –V measurements of the Au/ZnS-PVA/n-Si (MPS) structures were performed in the frequency and voltage ranges of 10–200 kHz and ±3 V at room temperature and are given in Figs. 3 and 4, respectively. As can be seen in these figures, three regions of inversion, depletion, and accumulation are clearly observed for each frequency such that this behavior matches with the behavior of a typical metal–insulator/oxide–semiconductor (MIS or MOS) type structure. As shown in Fig. 5, the value of C becomes almost constant and begins to decrease slowly with voltage due to the effect of R_s for sufficiently high frequencies between 1 V and 3 V (accumulation region/case) and then starts to decrease rapidly between 1 V and 0 V (depletion region), and finally, the value of C becomes almost constant or decreases slowly with applied bias voltage due to the effect of surface states between 0 V and −3 V (inversion region). Therefore, it can be said that the effect of R_s is prominent only accumulation region, but N_{ss} is effective both in depletion and inversion regions. For an ideal MIS diode in the accumulation case, no current flow through the structure and so the C–V plot becomes almost flat/constant or unchanged. Therefore, such behavior of C–V plot is close to the ideal case. On the other hand, in practice, the situation may be considerably different from the ideal case due to effects of surface states, series resistance of device, barrier homogeneity, and so on.

Because of the above explanations, for the microelectronic devices, admittance spectroscopy is an important nondestructive method for obtaining information on electrical and dielectric properties.[53–58] Usually, the value of C is independent of frequency in ideal case, but the situation is considerably different in applications due to N_{ss}, R_s , and native or deposited interfacial layer. As shown in Figs. 3 and 4, C–V and G/ω–V plots contain similar information on N_{ss} and R_s. Since the device is supplied with bias voltage or electric field, the N_{ss} levels move up or down with the valance and conductance bands while Fermi energy remains almost constant.[53–55] The higher values of the C and G/ω at low frequency (Figs. 3 and 4) were attributed to the excess capacitance (C_{ex}) and conductance (G_{ex}/ω) resulting from the N_{ss} in equilibrium with the n-Si since it could follow the alternating ac signal. These surface states usually may be created by the inter diffusion of atoms, dangling bonds and lattice defects, but the origin of R_s may arise from ohmic and rectifying contacts, the resistance of the quasi-neutral bulk semiconductor and extremely non-uniform doping distribution of donor or acceptor atoms.[56] While the values of C and G/ω at low frequency can be affected by R_s at higher frequencies especially in the accumulation region, they can be affected by N_{ss} both in inversion and depletion regions. The existence of interfacial layer at M/S interface can cause considerable deviations from the expected behavior of the ideal structures.[53–57] Contrary to low frequencies, the charge at the surface states or traps cannot follow the ac signal at high frequencies.

The variations on the G/ω–V characteristics (Fig. 6) verify the presence of various time-dependent responses of N_{ss}. The G/ω–V plots also have a distinctive peak due to N_{ss} and their relaxation time and the peak position shifts towards positive voltages with decreasing frequency.[56,58,59] It is clear that N_{ss} and R_s are the main reasons of the changes

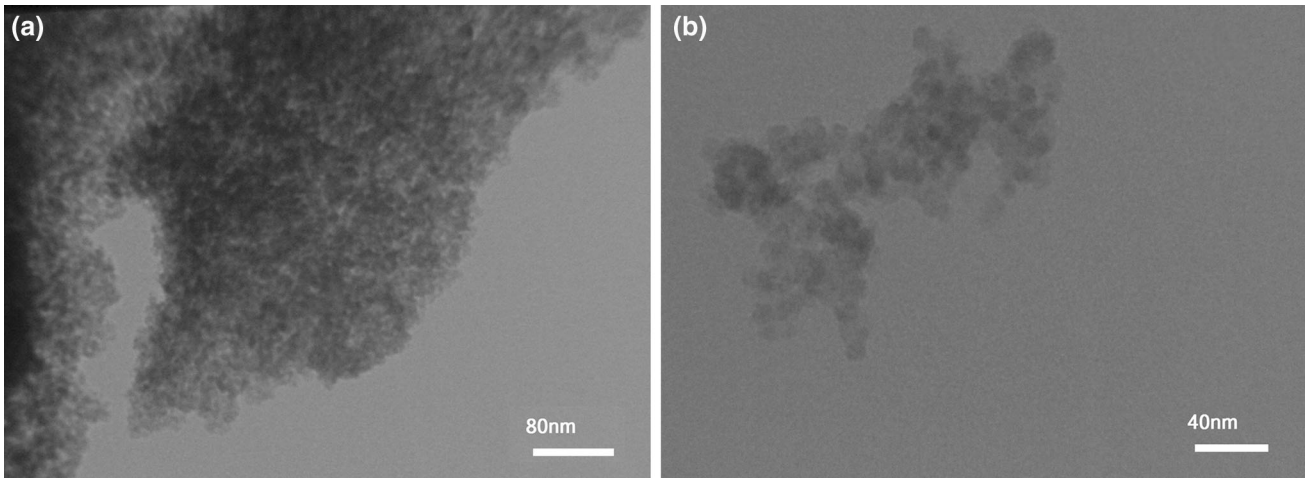

Fig. 3. (a, b) TEM image of as-prepared sample with 5% capping agent concentration with different magnifications.

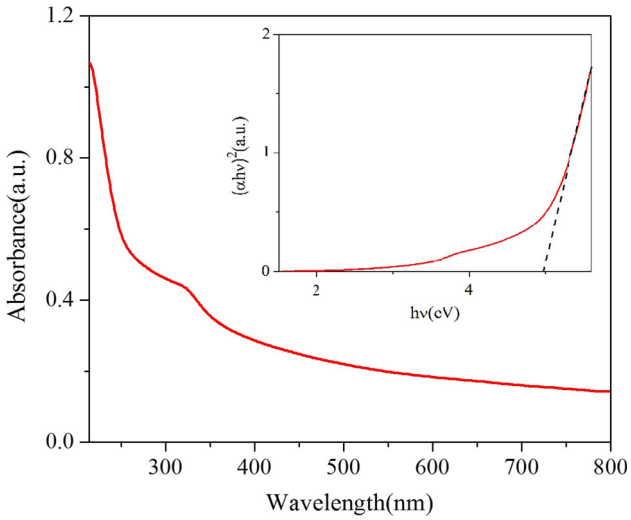

Fig. 4. UV–visible spectra and Tauc's plot of $(\alpha h\nu)^2$ against the photon energy ($h\nu$) for sample.

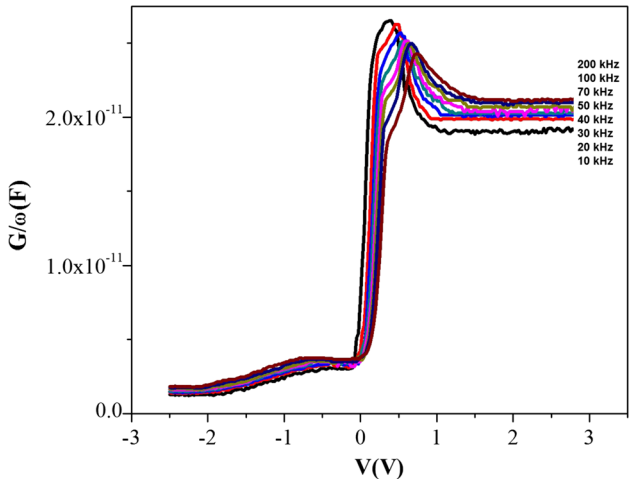

Fig. 6. Experimental forward and reverse bias G/ω–V characteristics of the Au/ZnS-PVA/n-Si (MPS) structure at various frequencies.

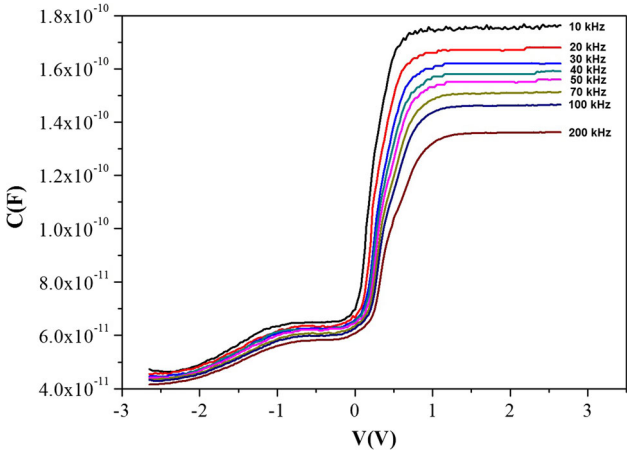

Fig. 5. Experimental forward and reverse bias C–V characteristics of the Au/ZnS-PVA/n-Si (MPS) structure at various frequencies.

in G/ω–V characteristics. At sufficiently high frequencies, N_{ss} cannot contribute to the capacitance and conductance as the charges at traps cannot fallow the ac signal, but the value of R_s becomes more effective on the C–V and G/ω–V plots and leads to error in the calculations. To avoid this error, general approach is the determine value of R_s and then apply it as an adjustment/correction to the measured C and G/ω values.

For the structure, the frequency and voltage dependent R_s can be calculated from the experimental C and G/ω measurements for each frequency as it can be seen in Eq. 2.[59] The real value of R_s is corresponding to strong accumulation region or sufficiently high forward biases for MIS, MOS, and MPS type structures. According to Nicollian and Brews,[59] the determination of R_s in both reverse and forward bias regions can be expressed as.[53,55,57,59]

$$R_S = \frac{G_m}{G_m^2 + (\omega C_m)^2} \tag{2}$$

where, C_m and G_m are the measured capacitance and conductance for any bias voltage and ($=2\pi/T$) is the angular frequency. Thus, the voltage dependent profile of R_s was calculated using C_m and G_m data in the frequency range of 10–200 kHz by using Eq. 2 and is given in Fig. 7. These very significant values demanded that special attention should be given to effects of the R_s in the application of the admittance-based measurement methods (C–V and G/ω–V). As seen in Fig. 5 the R_s–V plots exhibit a peak at about 0.1–0.4 V and it disappears at high frequencies due to the charges at surface states.[54–56] The magnitude of this peak increases with decreasing frequency and shift towards negative biases. In order to see and eliminate the effect of R_s on the measured C_m and G_m/ω the C_m–V and G_m/ω–V, plots (Figs. 3 and 4) were corrected using the following equations[59] and were given in Fig. 6a and b, respectively.

$$C_C = \frac{\left[G_m^2 + (\omega C_m)^2\right] C_m}{(\omega C_m)^2 + a^2} \tag{3}$$

$$G_C = \frac{\left[G_m^2 + (\omega C_m)^2\right] a}{(\omega C_m)^2 + a^2} \tag{4}$$

where

$$a = G_m - \left[G_m^2 + (\omega C_m)^2\right] R_s \tag{5}$$

The correction was made on the C–V plot for the effect of R_s, the values of the corrected C_c increases with increasing voltage in depletion region (Fig. 8a). On the other hand, the plot of the corrected G_c decreases with increasing voltage both in accumulation and inverse regions and also exhibits a distinctive peak due to surface states in equilibrium with semiconductor. It is clear that the values of R_s and interfacial layer are more effective especially in the accumulation region rather than N_{ss} and the effect of R_s can be eliminated at low frequencies.

The formation of barrier height (BH) between material semiconductor as well as its magnitude and nature are also very important on the electrical characteristics. Usually, in the inversion or weak depletion regions, C^{-2}–V plot has a linear behavior, and many diode parameters can be calculated from the intercept and slope of this linear region. In this region, the relationship between C and V in the inversion region can be expressed as.[55,57]

$$C^{-2} = \frac{2(V_R + V_0)}{q\varepsilon_s N_D A^2} \tag{6}$$

where V_R is the reverse bias voltage, N_D is the doping concentration of donor atoms and V_0 is the intercept voltage at zero bias which can be

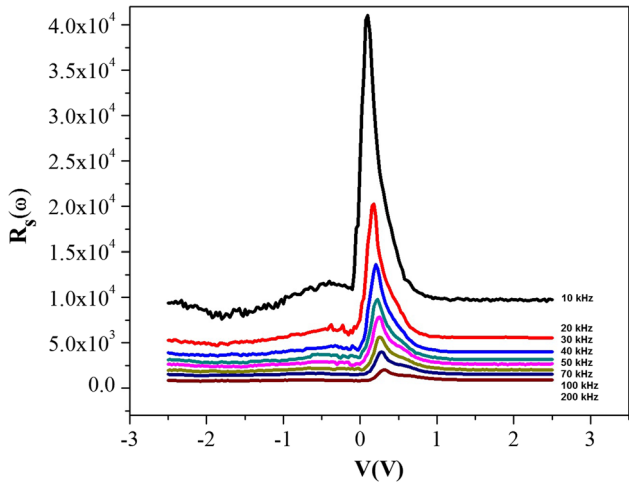

Fig. 7. The R_s–V plots of the Au/ZnS-PVA/n-Si (MPS) structure at various frequencies.

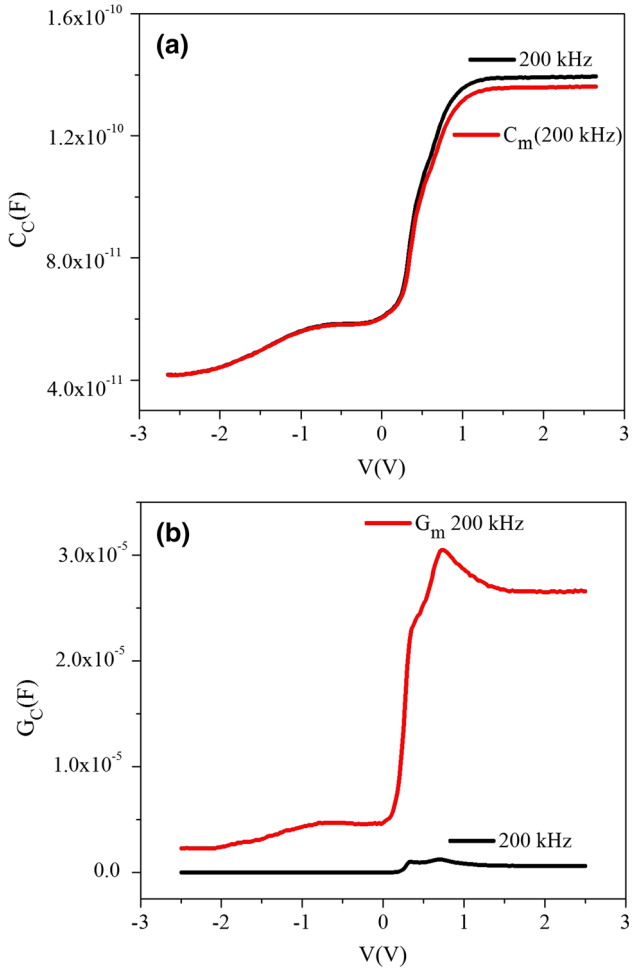

Fig. 8. The voltage dependent measured and corrected profiles of C and G plots (a) capacitance and (b) conductance of the Au/ZnS-PVA/n-Si (MPS) structure for 200 kHz.

determined from the extrapolation of the C^{-2}–V plot to the bias axis. The reverse bias C^{-2}–V plots of the Au/ZnS-PVA/n-Si (MPS) structure are presented for various frequencies (Fig. 9). As can be seen in this figure, C^{-2}–V plots exhibit a straight line in wide range of applied bias voltages for each frequencies. Thus, the value of N_D was obtained from the slope of the linear part of C^{-2}–V plot. The slope and intercept voltage of the C^{-2}–V plot are functions of interface layer. Thus, the values of Fermi energy level (E_F), and doping concentration atoms (N_D) were calculated at various frequencies from Fig. 7 using the following relations:

$$V_0 = V_D - \frac{kT}{q} \tag{7}$$

$$E_F = \frac{kT}{q}\ln\left(\frac{N_C}{N_D}\right) \tag{8}$$

The values of N_D were determined from the slope of the linear section of the C^{-2}–V characteristics (Fig. 7) for each frequency. The barrier height $\Phi_B(C$–$V)$ was calculated using the value of voltage intercept V_o of the C^{-2}–V plot at each frequency in the relation below:

$$\phi_B(C-V) = \left(V_0 + \frac{kT}{q}\right) + E_F = V_D + E_F \tag{9}$$

The obtained experimental values of the V_o, N_D, E_F, and $\Phi_B(C$–$V)$ are given in Table I. As it can be seen in Table I, the value of $\Phi_B(C$–$V)$ was found as 0.584 eV at 10 kHz and 0.764 eV at 200 kHz. At the same time, the value of N_D is 1.147×10^{15} cm^{-3} at 10 kHz while this value is 9.73×10^{14} cm^{-3} at 200 kHz. Such behavior can be entirely explained on the basis of the assumption that not all the surface states would follow the applied ac signal at sufficiently high frequencies.[54,58] Similar results have been reported in the literature by Tecimer et al.[55] and Yücedağ et al.[57] While the value of N_D decreases with increasing frequency, the value of $\Phi_B(C$–$V)$ increases as expected due to the effect of N_{ss} and polarization.

In order to determine the N_{ss} effects on the C–V and G/ω–V characteristics, the voltage dependent profiles of the N_{ss} were also obtained using low–high frequency capacitance (C_{LF}–C_{HF}) method by using following relation 10[54,56] and is given in Fig. 10.

$$N_{ss} = \frac{1}{qA}\left[\left(\frac{1}{C_{LF}} - \frac{1}{C_i}\right)^{-1} - \left(\frac{1}{C_{HF}} - \frac{1}{C_i}\right)^{-1}\right] \tag{10}$$

where A is the area of the rectifier/Schottky contact, q is the electronic change and C_i is the interfacial layer capacitance of the structure.

As shown in Fig. 8, N_{ss}–V plots have distinctive peaks in the depletion region due to the spatial distribution. Experimental results show that the effect of R_s and interfacial layer on the C–V and G/ω–V characteristics are remarkable at high frequencies. As shown in Fig. 8, the values of N_{ss} are very low and they are very suitable for an electronic device. These results confirmed that the value of N_{ss} may be passivized by the ZnS-PVA interfacial layer.

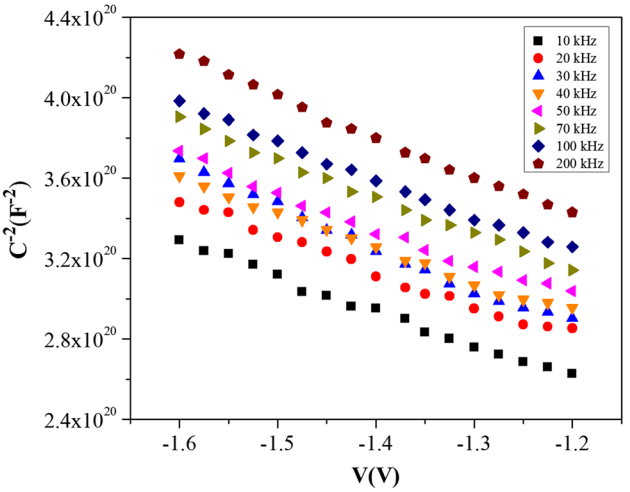

Fig. 9. The C^{-2}–V plots of the Au/ZnS-PVA/n-Si (MPS) structure at various frequencies.

Dielectric Properties

The ε', ε'', tan δ, M', and M'' values of Au/ZnS-PVA/n-Si (MPS) structure were investigated in detail by considering the effects of interfacial layer, polarization, surface states, and applied bias voltage or electric field. When interfacial layer R_s and N_{ss} are present, the applied bias voltage on the structure will be shared among them.[50,52,53] All of these parameters are significant in the electronic devices. The ε', ε'', tan δ', and M'' values were obtained from voltage and frequency dependent C and G data by using the following formulas, respectively.[57–59]

$$\varepsilon^* = \varepsilon' - j\varepsilon'' = Cd/A\varepsilon_o - j\,(Gd/\omega A\varepsilon_o) \tag{11}$$

$$\tan\delta = \varepsilon''/\varepsilon' \tag{12}$$

$$M^* = \frac{1}{\varepsilon^*} = M' + jM'' = \frac{\varepsilon'}{\varepsilon'^2 + \varepsilon''^2} + j\frac{\varepsilon''}{\varepsilon'^2 + \varepsilon''^2} \tag{13}$$

where j is the imaginary root of -1, A is rectifier contact area in cm^2, d is the thickness of the interfacial layer, ε_o (=8.85×10^{-14} F/cm) is the permittivity of free space. Figure 9 shows the voltage-dependent values of the ε' curves of the structures at various frequencies

As shown in Fig. 11, ε' was found to be a strong function of voltage and frequency especially in the depletion and accumulation regions and its value increases as the frequency is decreased. The change in the ε'–V plot with frequency can be related to Maxwell–Wagner and space charge polarization.[53,57,60] Especially at low frequencies, localized charge dipole and surface states can easily follow

Table I. The obtained experimental values of the V_o, N_D, E_F and Φ_B(C–V) electrical parameters of the Au/ZnS-PVA/n-Si (MPS) structure at various frequencies at 300 K

f (kHz)	V_o (eV)	N_D (cm^{-3})	V_D (eV)	E_F (eV)	Φ_B (C–V) (eV)
10	0.323	1.147×10^{15}	0.349	0.235	0.584
20	0.421	1.143×10^{15}	0.447	0.235	0.682
30	0.464	9.597×10^{14}	0.489	0.234	0.698
40	0.527	1.157×10^{15}	0.552	0.235	0.787
50	0.511	1.121×10^{15}	0.536	0.236	0.772
70	0.504	1.058×10^{15}	0.529	0.237	0.766
100	0.568	1.068×10^{15}	0.593	0.237	0.830
200	0.499	9.730×10^{14}	0.525	0.240	0.764

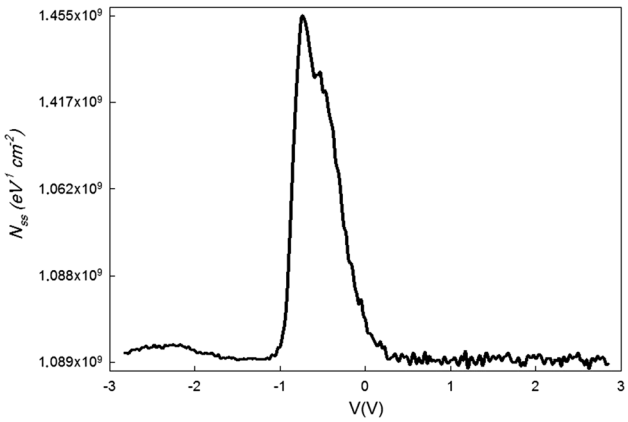

Fig. 10. The experimental N_{ss}–V profile of the Au/ZnS-PVA/n-Si (MPS) structure obtained from the C_{LF}–C_{HF} frequency capacitance method.

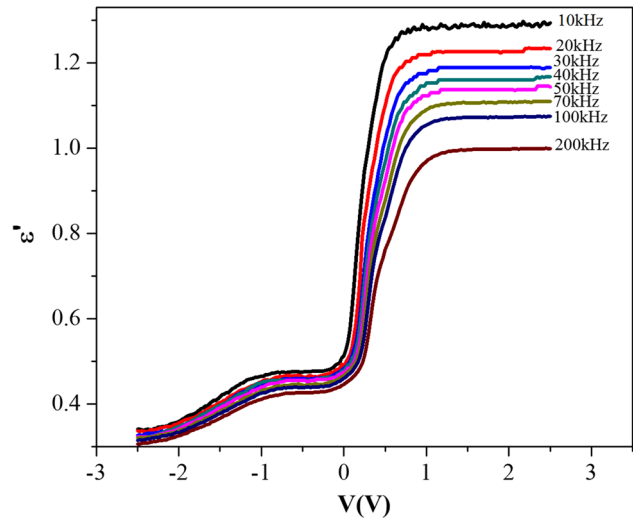

Fig. 11. Experimental ε'–V plots of the Au/ZnS-PVA/n-Si (MPS) structure at various frequencies.

the ac signal and contribute to both the real and imaginary parts of the dielectric constant values.[57,60]

The ε''–V plots of Au/ZnS-PVA/n-Si structure (Fig. 12) also show similar behavior with ε'–V plots and they exhibit a peak in the accumulation region such that the peak magnitude decreases with increasing frequency. The peak position shifts toward higher positive voltage region with increasing frequency due to the surface and dipole polarizations and N_{ss} under external electric field. Under electric field, surface states can be restructured and reordered. The magnitude of dielectric parameters especially depends on the interfacial effect within bulk of the sample, interfacial layer, surface states, surface polarization, and electrode effect.[53–57]

The values of tan δ of Au/ZnS-PVA/n-Si structure as a function of voltage in the frequency range of 10–200 kHz are given in Fig. 13. The tan δ–V plots of the structures (Fig. 13) exhibit also an anomalous peak behavior both in inversion and depletion regions depending on ε' and ε'' values.[61] The peak values of tan δ–V decreased with increasing frequency and the peak positions slightly shift towards inversion region due to restructuring and reordering of N_{ss} under external dc electric field. Also, it is

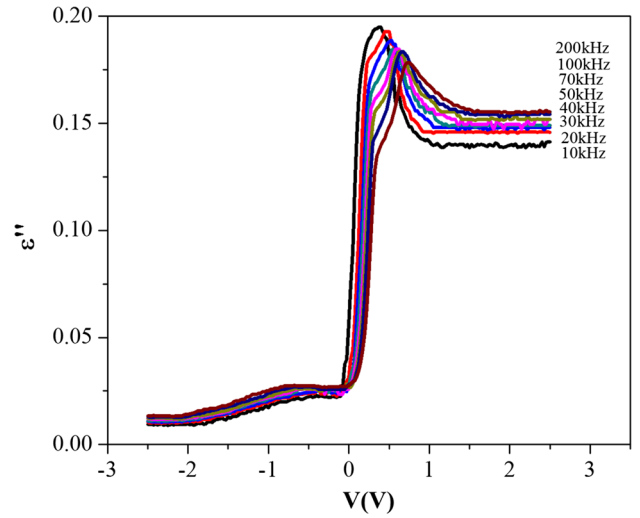

Fig. 12. Experimental ε''–V plots of the Au/ZnS-PVA/n-Si (MPS) structure at various frequencies obtained from G/ω–V plot.

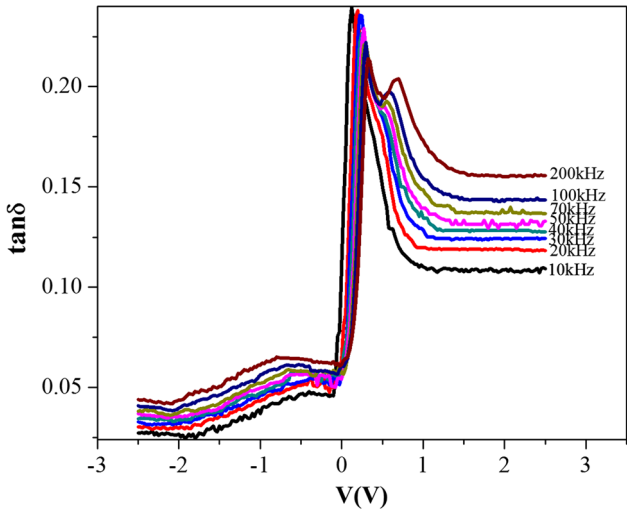

Fig. 13. The variations of dielectric loss versus applied voltage for various frequencies of Au/ZnS-PVA/n-Si (MPS) structure.

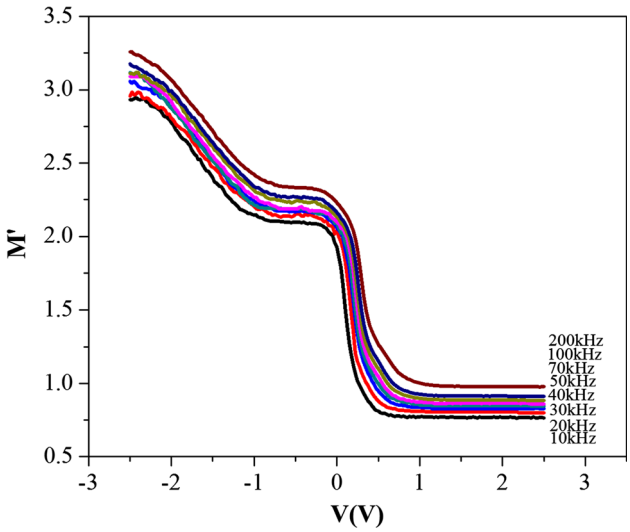

Fig. 14. The frequency dependence of the real part (M') of complex electric modulus (M^*) of Au/ZnS-PVA/n-Si (MPS) structure.

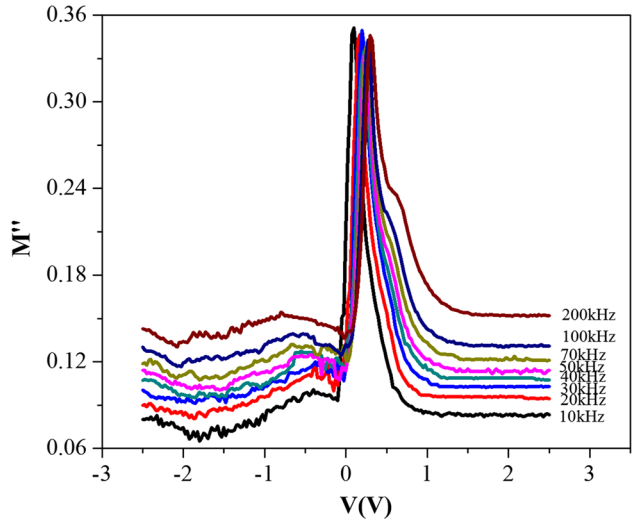

Fig. 15. The frequency dependence of the imaginary part (M'') of complex electric modulus (M^*) of Au/ZnS-PVA/n-Si structure.

well known that the C and G/ω are extremely sensitive to the interface properties and R_s of the structure.[54,61] The obtained experimental tan δ–V plots have confirmed that the values of N_{ss} and interfacial polarization are effective when bias voltages are applied. Similar results have been reported in the literature,[62] and such peak behavior was ascribed to only interface states. Electric modulus formalism offers some advantages in the interpretation of bulk relaxation phenomena in complex systems.[57–61] Thus, the evaluation of the electric modulus as a function of frequency permits one to detect the presence of relaxation processes in the studied materials. M'–V plots are also obtained by using $\varepsilon'$and ε'' data for various frequencies and given in Fig. 14. As can be seen in Fig. 12 the value of M' decreases with increasing voltage while increases slightly with increasing frequency. The features of M'–V plots are attributed to the relaxation, polarization in doped insulator and charges in traps.[60–62] Also the existence of charges in traps gives rise to interfacial polarization.[61]

Figure 15 shows the frequency dependence of the imaginary (M'') part of the complex electric modulus (M^*) of the Au/ZnS-PVA/n-Si structure. As shown in Fig. 13 M'' is a strong function of frequency and applied bias voltage and it increases with increasing frequency almost in the whole applied bias voltage range. M'' values exhibit an anomalous peak and the magnitude of this peak slightly increases with decreasing frequency owing to the contribution to the interface trap charges and similar results have been reported in the literature.[54,55,61,62] It is clear that tan δ is in close relation with the conductivity. The alternating current (ac) conductivity σ_{ac} is calculated using the relation below.[53]

$$\sigma_{ac} = 2\pi f \varepsilon_0 \varepsilon' \tan\delta \qquad (14)$$

Figure 16 shows the behavior of ac conductivity (σ_{ac}) with voltage at various frequencies ranging from 10 kHz to 200 kHz. It is clear that the value of the σ_{ac} almost increases with increasing voltage and frequency due to the decreasing polarization with increasing frequency.[61–63] The increase in electrical conductivity leads to an increase in the eddy current which in turn increases the energy loss tan δ.[64] Similar behavior was observed in the literature by Afendiyava et al.,[65] who explained the increase in σ_{ac} with increasing frequency by the gradual decrease in R_s.

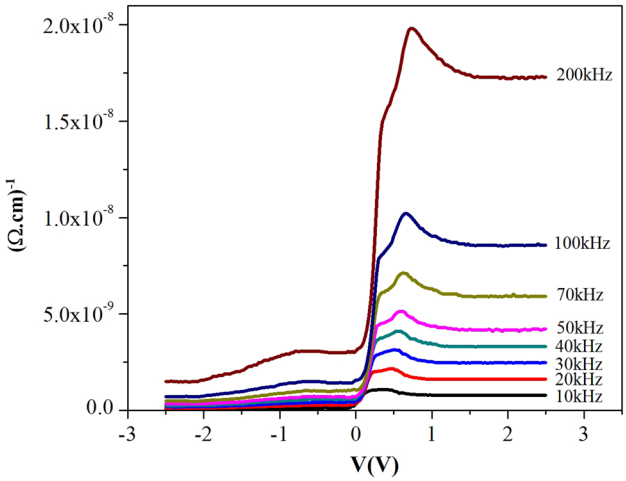

Fig. 16. Frequency dependence of the ac electrical conductivity (σ_{ac}) for various frequency of Au/ZnS-PVA/n-Si (MPS) structure.

CONCLUSION

The frequency and voltage dependence of electrical and dielectric properties of the fabricated Al/ZnS-PVA/n-Si (MPS) structures were investigated in detail using C–V and G/ω–V measurementsin the frequency and voltage ranges of 10–200 kHz and ±3 V, respectively, at room temperature. The electrical and dielectric properties of the MPS structure was determined as function of frequency and applied bias voltage by considering the effect of R_s, N_{ss} and interfacial layer. C–V and G/ω–V plots of Au/ZnS-PVA/n-Si (MPS) type structure for each frequency clearly exhibit inversion, depletion and accumulation regions like a metal–insulator–semiconductor (MIS) structure and their values decrease with increasing frequency for each region. While these discrepancies in the C–V and G/ω–V plots at inversion and depletion regions were attributed to surfaces states (N_{ss}), interfacial and dipole polarization, the discrepancies of same plots at accumulation region were attributed to R_s and interfacial ZnS-PVA layer. Firstly, main electrical parameters of the MPS structure such as the N_D, V_D, E_F , and $\Phi_B(C$–$V)$ were obtained from the reverse bias C^{-2}–V plots for each frequency. The value of N_D decreases with increasing frequency, whereas the value of $\Phi_B(C$–$V)$ increases as expected due to the effect of N_{ss} and polarization. In order to determine the effects of R_s and N_{ss} on the C–V and G/ω–V characteristics, the voltage dependent profile of the R_s and N_{ss} of the structure were also obtained using admittance and low–high frequency methods, respectively. R_s–V and N_{ss}–V plots, both, revealed distinctive peaks in the depletion region due to the spatial distribution. The peak observed in the R_s–V plot was attributed to the spatial distribution of N_{ss} at interfacial layer/semiconductor interface and the magnitude of peak decreases with increasing frequency. Experimental results show that the effect of R_s and interfacial layer on the C–V and G/ω–V characteristics are remarkable at high frequencies. Therefore, the high frequency C–V and G/ω–V *plots* were corrected to eliminate the effect of R_s. Secondly, main dielectric parameters such as ε', ε'', M', M'', tan δ, and σ_{ac} were also obtained from the measured C and G/ω data and it was seen that these parameters are strong functions of frequency and bias voltage. All of experimental results confirmed that N_{ss}, R_s and interfacial layer of the MPS structure are quite important parameters, which strongly influence both the electric and dielectric properties. In conclusion, the low values of Nss ($\sim 10^9$ eV^{-1} cm^{-2}) and the value of dielectric constant ($\varepsilon' = 1.3$) of ZnS-PVA interfacial layer even at 10 kHz are very suitable for electronic devices when compared to the SiO_2. These results confirmed that the ZnS-PVA has considerably improved the performance of Au/n-Si (MS) structure while attaining the property of a capacitor which stores electric charges or energy. In addition, the C–V plot of the fabricated Au/ZnS-PVA/n-Si (MPS) structure is close to the ideal MIS type SBD behavior. As can be seen in figures, the C–V plots do not have a large fluctuation in inversion and accumulation regions due to the low values of N_{ss} and R_s.

REFERENCES

1. M. Khatami, S. Pourseyedi, M. Khatami, H. Hamidi, M. Zaeifi, and L. Soltani, *Biores. Bioprod. (BRBP)* 2, 1 (2015).
2. M. Jayandran, M.M. Haneefa, and V. Balasubramanian, *J. Chem. Pharm. Res.* 7, 251 (2015).
3. R.M. Agrawal, S.D. Charpe, F.C. Raghuwanshi, and G.T. Lamdhade, *Int. J. Appl. Innov. Eng. Manag. (IJAIEM)* 4, 141 (2015).
4. G. Anandha Babu, G. Ravi, Y. Hayakawa, and M. Kumaresavanji, *J. Magn. Magn. Mater.* 375, 184 (2015).
5. T. Ali and A. Venkataraman, *Int. J. Adv. Eng. Technol.* 7, 122 (2014).
6. M. Kooti and L. Matturi, *Int. Nano Lett.* 1, 38 (2011).
7. D. Moore and Z.L. Wang, *J. Mater. Chem.* 16, 3898 (2006).
8. B. Bodo, R. Singha, and S.C. Das, *Int. J. Appl. Phys. Math.* 2, 287 (2012).
9. R. John and S.S. Florence, *Chalcogenide Lett.* 7, 263 (2010).
10. D. Ayodhya, M. Venkatesham, A.S. Kumari, K.G. Mangatayaru, and G. Veerabhadram, *J. Appl. Chem.* 6, 1 (2013).
11. T.T.Q. Hoa, L. Van Vu, T.D. Canh, and N.N. Long, *J. Phys. Conf. Ser.* 187, 1 (2009).
12. N.K. Abbas, K.T. Al-Rasoul, and Z.J. Shanan, *Int. J. Electrochem. Sci.* 8, 3049 (2013).
13. K.V. Anand, R. Mohan, R.M. Kumar, M.K. Chinnu, and R. Jayavel, *Proc. Indian Natl. Sci. Acad.* 79, 395 (2013).
14. M. Hafeez, U. Manzoor, and A.S. Bhatti, *J. Mater. Sci. Mater. Electron.* 22, 1772 (2011).
15. U. Gangopadhyay, K. Kyunghea, S.K. Dhungel, D. Mangalaraj, J.H. Park, and J. Yi, *Trans. Electr. Electronic Mat.* 5, 1 (2004).
16. A. Chandran, N. Francis, T. Jose, and K.C. George, *SB Acad. Rev.* 7, 17 (2010).
17. M. Sookhakian, Y.M. Amin, W.J. Basirun, M.T. Tajabadi, and N. Kamarulzaman, *J. Lumin.* 145, 244 (2014).
18. J.P. Borah and K.C. Sarma, *Acta Phys. Pol. A* 114, 713 (2008).
19. A.K. Thottoli and A.K.A. Unni, *J. Nanostruct. Chem.* 3, 56 (2013).

20. X. Li, X. Wang, Q. Xiong, and P.C. Eklund, *Nano Lett.* 5, 1982 (2005).
21. X. Wang, H. Huang, B. Liang, B. Liu, D. Chen, and G. Shen, *Solid State Mater. Sci.* 38, 57 (2013).
22. M. Ahmad, K. Rasool, M.A. Rafiq, M.M. Hasan, C.B. Li, and Z.A.K. Durrani, *Phys. E* 45, 201 (2012).
23. C. Lawther and J. Woods, *J. Lumin.* 18 & 19, 724 (1979).
24. S.-P. Han, H. Ko, J.-W. Park, N. Kim, Y.-J. Yoon, J.-H. Shin, D.Y. Kim, D.H. Lee, and K.H. Park, *Opt. Express* 21, 25875 (2013).
25. T.F. Kuech and J.O. McGaldin, *J. Vac. Sci. Technol.* 17, 891 (1980).
26. D. Korucu and A. Turut, *Int. J. Electron.* 101, 1595 (2014).
27. Ç. Bilkan, Y. Azizian-Kalandaragh, Ş. Altındal, and R. Shokrani-Havigh, *Phys. B Condens.* 500, 154 (2016).
28. A.R. Deniz, Z. Caldiran, Y. Sahin, M. Sinoforoglu, O. Metin, K. Meral, and S. Aydogan, *Met. Mater. Trans. A* 44, 3813 (2013).
29. B. Kinaci, Y. Ozen, K. Kizilkaya, T. Asar, S.S. Cetin, E. Boyali, and S. Ozcelik, *J. Mater. Sci. Mater. Electron.* 24, 1375 (2013).
30. D. Korucu and S. Duman, *Thin Solid Films* 531, 436 (2013).
31. G. Ersöz, İ. Yucedağ, Y. AzizianKalandaragh, İ. Orak, and Ş. Altıdal, *IEEE Trans. Electron Devices* 63, 2948 (2016).
32. Y. Lv, Z. Lin, T.D. Corrigan, J. Zhao, Z. Cao, L. Meng, C. Luan, Z. Wang, and H. Chen. *J. Appl. Phys.* 109, 074512 (2011).
33. A. Kumar, T. Kumar, A. Hahnel, D. Kanjilal, and R. Sing, *J. Appl. Phys.* 104, 1 (2014).
34. İ. Yücedağ, G. Ersöz, A. Gümüş, and Ş. Altındal, *Int. J. Mod. Phys. B* 29, 1550075 (2015).
35. L. Vafayi, S. Gharibe, and S. Afshar, *J. Appl. Chem. Res.* 7, 63 (2013).
36. E.K. Goharshadi, S.H. Sajjadi, R. Mehrkhah, and P. Chem, *Eng. J.* 209, 113 (2012).
37. H.V. Chung, P.T. Huy, T.T. An, N.T.M. Thuy, and N.D. Chien, *J. Korean Phys. Soc.* 52, 1562 (2008).
38. J.L. Yuan, K. Kajiyoshi, K. Yanagisawa, H. Sasaoka, and K. Nishimura, *Mater. Lett.* 60, 1284 (2006).
39. J.P. Borah, J. Barman, and K.C. Sarma, *Chalcogenide Lett.* 5, 201 (2008).
40. D.C. Onwudiwe and P.A. Ajibade, *Int. J. Mol. Sci.* 12, 5538 (2011).
41. Q. Zhao, L. Hou, and R. Huang, *Inorg. Chem. Commun.* 6, 971 (2003).
42. G. Nabiyouni, R. Sahraei, M. Toghiany, M.H. Majles Ara, and K. Hedayati, *Rev. Adv. Mater. Sci.* 27, 52 (2011).
43. X. Cheng, Q. Zhao, Y. Yang, S.C. Tjong, and R.K.Y. Li, *J. Mater. Sci.* 45, 777 (2010).
44. M. Dela Garza, I. Lopez, F. Avina, and I. Gomez, *J. Ovonic Res.* 9, 89 (2013).
45. T. Prakash, R. Jayaprakash, G. Neri, and S. Kumar, *J. Nanopart.* 2103, 1 (2013).
46. I. Taşcıoğlu, W.A. Farooq, R. Turan, S. Altındal, and F. Yakuphanoğlu, *JALCOM* 590, 157 (2014).
47. F. Yakuphanoğlu, A. Tataroğlu, A. Al-Ghmadi, R.K. Gupta, Y. Al-Turki, Z. Şerbetçi, S. BinOmran, and F. El-Tantawy, *Sol. Energy Mater. Sol. Cells* 133, 699 (2015).
48. S.A. Yerişkin and H.I. Unal, *J. Appl. Polym. Sci.* 120, 390 (2011).
49. A. Tabip, N. Sdiri, H. Elhouichet, and M. Ferid, *JALCOM* 622, 687 (2015).
50. Y.Ş. Asar, T. Asar, S. Altındal, and S. Özçelik, *JALCOM* 628, 442 (2015).
51. S. Zeyrek, E. Acaroğlu, S. Altındal, S. Birdoğan, and M.M. Bülbül, *Curr. Appl. Phys.* 13, 1225 (2013).
52. R. Padma, B. Prasanna, and V. Rajagopal Reddy, *Superlattices Microstruct.* 60, 358 (2013).
53. V. Rajagopal Reddy, *Thin Solid Films* 556, 300 (2014).
54. S. Demirezen, A. Kaya, Ş. Altıdal Yerişkin, M. Balbaşı, İ. Uslu, *Results in Phys.* 6, 180 (2016).
55. H. Tecimer, H. Uslu, Z.A. Alahmed, and F. Yakuphanoğlu, *Compos. B* 57, 25 (2014).
56. Y. Azizian-Kalandaragh, U. Aydemir, and S. Altındal, *J. Electron. Mater.* 43, 1226 (2014).
57. İ. Yücedağ, A. Kaya, Ş. Altındal, and I. Uslu, *China Phys. B* 23, 047304 (2014).
58. A. Turut, A. Karabulut, K. Ejderha, and N. Bıyıklı, *Mater. Sci. Semicond. Process.* 39, 400 (2015).
59. E.H. Nicollian and J.R. Brews, *Metal Oxide Semiconductor (MOS) Phys. and Tech.* (New York: Wiley, 1982).
60. P.B. Macedo, C.T. Moyniham, and R. Bose, *Phys. Chem. Glass* 13, 171 (1972).
61. İ. Yücedağ, A. Kaya, and Ş. Altındal, *Int. Mod. Phys. B* 28, 1450153 (2014).
62. İ. Yücedağ, A. Kaya, H. Tecimer, and Ş. Altındal, *Mater. Sci. Semicond. Process.* 28, 37 (2014).
63. O. Bidault, P. Goux, M. Kchikech, M. Belkaoumi, and M. Maglion, *Phys. Rev. B* 49, 7868 (1994).
64. İ.M. Afendiyeva, I. Dökme, S. Altındal, M.M. Bülbül, and A. Tataroglu, *Microlectron. Eng.* 85, 247 (2008).
65. İ. Yücedağ, Ş. Altındal, and A. Tataroğlu, *Microlectron. Eng.* 84, 180 (2007).